Available online at www.sciencedirect.com

SciVerse ScienceDirect

Journal of the European Ceramic Society 32 (2012) 2443–2450

www.elsevier.com/locate/jeurceramsoc

Nanosecond reversible solid state switches capable of handling MJ of energy

Renaud Metz [a,b,*], Julien Pansiot [a], Mehrdad Hassanzadeh [c]

[a] Institut Charles Gerhardt Montpellier, UMR 5253 CNRS, Université Montpellier 2, ENSCM, 8, Rue de l'Ecole Normale, 34296 Montpellier Cedex 05, France
[b] Laboratoire Matériaux Energétiques et Composés Polyazotés, Lyon1-CNRS-Isochem (groupe SNPE), UMR 5179 CNRS/UCBL/CNES/SNPE, Université Claude Bernard – Lyon 1, Batiment Berthollet, 69622 Villeurbanne Cedex, France
[c] Schneider Electric, Medium Voltage Switchgear Business, DRC, 1340 Rue de Pinville, 34965 Montpellier Cedex 2, France

Received 19 May 2011; received in revised form 26 January 2012; accepted 28 January 2012
Available online 25 February 2012

Abstract

The theoretical applicability of the Schottky thermionic emission model to electronic transport at tin dioxide grain boundaries is addressed. Firstly, the theoretical behaviour of the barrier height $\phi_{(v)}$ versus applied voltage V is determined for a single grain boundary. Next we predict the current density–voltage characteristics as a function of temperature, demonstrating good correlation between experimental and theoretical results. The model carried out has the advantage that it contains no adjustable parameters. Agreement with experimental results from optimised polycrystalline ceramics gives strong evidence for the double-depletion-layer/thermionic-emission model. Moreover, this study emphasises the importance of the direct large-bandgap of doped SnO_2 in surge-arrester applications, and gives credibility to the analogy between the apparent behaviour of doped SnO_2 and doped ZnO varistors. Doped polycrystalline tin oxide ceramic is the first material to compete with doped ZnO in the medium and high voltage applications for surge arresters.

Keywords: SnO_2; Varistor; Surge arrester

1. Introduction

Varistors are nowadays currently used as voltage spike suppressors in electronic, electro-technical and tactical devices. The word varistor comes from a portmanteau of the words variable and resistor. It is a passive component that displays a non-ohmic, current–voltage behaviour, which may be used as clamping device to limit a voltage to defined level.[1] Commercial varistors are based on both SiC and ZnO, in spite of the fact that ZnO exhibits substantially and indisputably higher performances. Recently in 1995[2] SnO_2-based ceramics have found new applications as varistors, although studies on the electrical properties of such non-linear semiconductor devices were already underway in Russia in the early 1970s.[3] More than 300 scientific papers, all devoted to doped SnO_2 varistors, have been since published. (SciFinder bibliography analysis over the period 1995–2009.)

In ZnO varistors, the so-called varistor effect is controlled electrically by grain boundaries that are tuned by composition, microstructure and sintered material processing. The model of Greuter et al.[4–7] offers a good description of the highly non-linear properties of the electrically active grain boundaries of correctly doped and manufactured ZnO ceramics. The essential principle underlying varistor action relies on an analogy between the electronic behaviour of a ceramic grain boundary and a metal–semiconductor junction.

The metal–semiconductor (M-SC) junction is the simplest unipolar device at the base of a great number of more complex structures. In this type of device, only one type of particle (electron or hole) assumes the role of charge carrier and determines the operating conditions of the device. Generally, application of a potential difference across M-SC junction produces a non-symmetrical I–V characteristic, which is useful in semiconductor electronics applications such as Schottky diodes. In actual fact, however Schottky barriers appear at most semiconductor interfaces: solid–air interface or grain boundaries. The Schottky barrier corresponds to the energy barrier to which a

* Corresponding author at: Laboratoire Charles Coulomb (L2C-CVN-Equipe Nanostructures), UMR CNRS 5221, Bâtiment 11, Place E. Bataillon, 34095 Montpellier Cedex 5, France.Tel.: +33 4 67 14 40 64.
E-mail addresses: renaud.metz@univ-montp2.fr, renaud.metz@univ-lyon1.fr (R. Metz).

0955-2219/$ – see front matter © 2012 Elsevier Ltd. All rights reserved.
doi:10.1016/j.jeurceramsoc.2012.01.029

free electron moving towards the semiconductor is confronted. The origin of theses electrostatic barriers at the interfaces stems from lattice mismatches, defect concentration and dopant segregation at the grain surface and/or grain boundary. In the case of grain boundaries, the electrical behaviour is symmetrical and can be described as two Schottky barriers connected back-to-back.

However in the specific case of both ZnO and SnO_2, an unexpectedly high level of non-linearity and a high-energy handling capability are observed. The last property is due to the ceramic polycrystalline microstructure, although the physical origin is yet not very well understood.[1,8,9] Concerning the non-linearity performance, values of α up to 100 have been reported.[1,10]

The first high voltage investigations have been released recently.[11,12] These first studies produced encouraging results, but need to be improved to compete with ZnO polycrystalline material. The purpose of this study is to report both on one of the best formulations obtained so far and to give, for the first time, a comprehensive thermionic emission model applied to an electrically active grain boundary in doped SnO_2.

2. Experimental

The oxides used in this study were SnO_2 (Alfa Aesar, 99.9%), Co_3O_4 (Alfa Aesar, 99.7%), Nb_2O_5 (Aldrich, 99.9%), Cr_2O_3 (Alpha Aesar, 99%), B_2O_3 (Alfa Aesar, 99.98%), Ta_2O_5 (Aldrich, 99.99%), Tl_2O_3 (Fluka, 99%) and Al_2O_3 (Aldrich, 98%).

The oxides were mixed in appropriate proportions and ball-milled in agate bottles for 1 h.

The oxide powders were then mixed with a polyvinyl alcohol binder granulated and pressed into pellet shapes. The powders were uniaxially constrained at a pressure of 7×10^9 Pa during few seconds. Pellets with a diameter of about 10 mm and a thickness of about 2 mm were then sintered in ambient air atmosphere at 1623 K for 2 h. They were heated at a rate of 120 K h^{-1} to the sintering and room temperatures. Densities were determined by geometrical measurement of the volume and by weighing the pellets using an analytical balance. The relative density of the specimens was calculated starting from the following formula:

$$\text{Relative density}\,(\%) = 100\frac{\rho}{\rho_{th}} \quad (1)$$

with ρ = apparent density of the pellet (g cm^{-3}), $\rho_{th} = 6.95$ g cm^{-3}; theoretical density of SnO_2 calculated from a tetragonal SnO_2 structure with cell parameters: $a = 0.4738$ nm and $c = 3.185$ nm.[13]

Microstructure characterisation of sintered samples was made by scanning electron microscopy (Hitachi S 800 and XL30 ESEM Philips coupled with energy dispersive spectroscopy (EDS – EDAX)). X-ray patterns on ground sintered ceramics were recorded on a Bruker D8 Advance diffractometer ($CuK_{\alpha 1,\alpha 2}$) equipped with a Vantec detector and a spinner.

The average size of the grains was measured by Mendelson's method[14] as per the recommended formula: $G = 1.56\,L$, with L: the average length between grains.

For the electrical measurements, silver contacts were deposited on the sample surfaces, after which the pellets were heat-treated at 873 K for several minutes. To determine the electrical properties as a function of temperature a special sample holder was built and attached to an electrical source and two digital multimeters for current higher than 1 mA cm^{-2}, the current–voltage measurements were taken using a high voltage-measuring unit using a current generator which delivers a 8/20 μs impulse current with a peak short-circuit of 6 kA. The non-linear coefficient was obtained by linear regression of the experimental points using a logarithmic scale around 1 mA cm^{-2} and the breakdown electrical field was calculated at this current density. The non-linear coefficient α, for all the samples studied, was estimated between two desired magnitudes of current and corresponding voltage by

$$\alpha = \log_{10}\left(\frac{E_{1\text{mAcm}^{-2}}}{E_{0.1\text{mAcm}^{-2}}}\right) \quad (2)$$

where $E_{0.1\text{mAcm}^{-2}}$ and $E_{1\text{mAcm}^{-2}}$ stand for the voltage fields at current densities 0.1 mA cm^{-2} and 1 mA cm^{-2}, respectively.

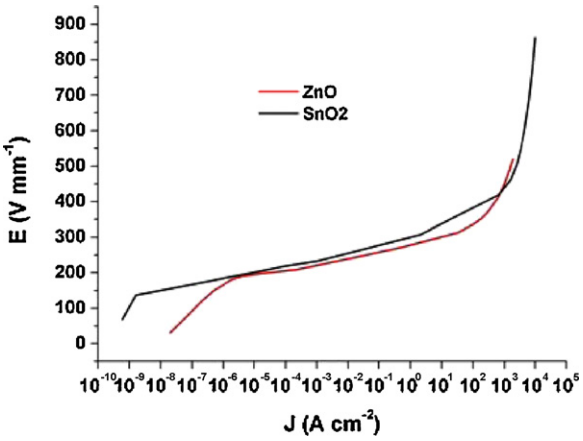

Fig. 1. Electric field according to the current density for doped dioxide varistors sintered at 1350 °C during 2 h after a cooling of 120 K h^{-1}. For comparison purpose the electrical behaviour of a doped-ZnO commercial ceramic is reported.

3. Results and discussion

3.1. Electronic parameters describing the potential barrier at the grain boundary

After many empirical tests on ceramic formulations that foster on both large non-linearity coefficient and absorption capability we found that the composition [97.7145%$_{wt}$ SnO_2 + 0.5355%$_{wt}$ Co_3O_4 + 0.5%$_{wt}$ Nb_2O_5 + 0.25%$_{wt}$ Cr_2O_3 + 0.1%$_{wt}$ B_2O_3 + 0.25%$_{wt}$ Ta_2O_5 + 1%$_{wt}$ $Tl(NO_3)_3$, $3H_2O$ + 0.05%$_{wt}$ $Al(NO_3)_3$, $9H_2O$] exhibits the largest range of operation. As depicted in Fig. 1, current density versus applied field E, there is an enormous variation in current (a factor of 10^{12}: 10^{-9} to 10^3 A cm^{-2}) while the applied field varies only about a factor of 3 (150–400 V mm^{-1}).

By conducting the electric tests and knowing the microstructure, we can estimate a potential barrier per grain. In fact, if we accept that ceramics are homogeneous with grains of the same

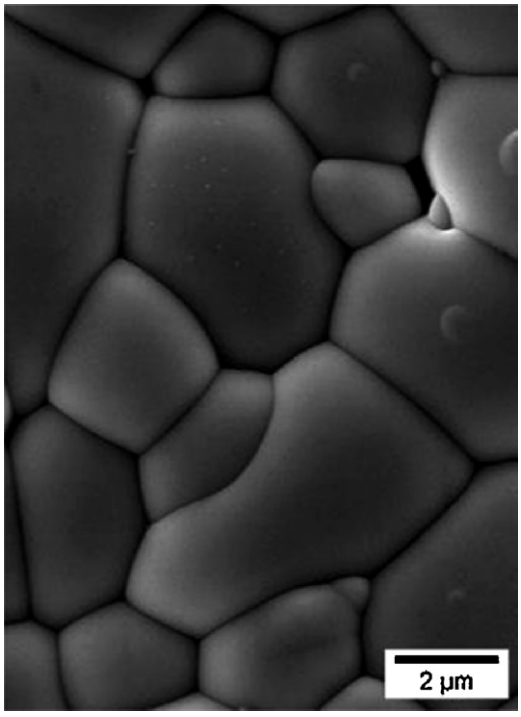

Fig. 2. SEM micrographs of typical microstructure of doped-SnO_2 ceramics sintered at 1623 K for 2 h.

size ($G = 12 \times 10^{-3}$ mm – Fig. 2) the voltage of a single grain boundary (V_{gb}) is given as

$$V_{gb} \sim 12 \times 10^{-3}\, E_{1mAcm^{-2}} \quad (3)$$

Table 1 shows the breakdown voltage per grain boundary (V_{gb}) measured on bulk sample. This value, ~3 V, is expected to be lower than the true breakdown voltage per grain. This follows since the current always seeks the easiest path. Hence the number of grains for the current path is actually lower than the average number of grains between the electrodes. Microscopic data on current–voltage characteristics of a single grain boundary has been recently reported as 5.2–5.5 V at current 50 µA.[15] Our data therefore appear to be in agreement with the result of this previous study.

Despite an unsatisfactory model to describe electrical conduction in SnO_2 varistors,[16] purely thermionic conduction mode, i.e. electron emission from the localised grain-boundary states to the conduction band, the values of voltage barrier height and donor concentration are reasonable. From the extrapolation at $E = 0$ of $\mathrm{Ln}\, J = f(E^{1/2})$ we estimate the height of the potential barrier at the grain boundaries. The experimental measures were carried out in the pA range (10^{-12} A). The value of the potential barrier height (Φ_0) was estimated as follows:

$$\ln\ (j) - \frac{(\beta E^{1/2} - \phi_0)}{kT} + \ln\ (AT^2) \quad (4)$$

$$\ln(j_{E=0}) = \ln(AT^2) - \frac{\phi_0}{kT} \Leftrightarrow \phi_0 = kT[\ln(AT^2) - \ln(j_{E=0})] \quad (5)$$

where A denotes the effective Richardson's constant. The effective Richardson's constant is a materials constant defined as $A = 4\pi m * k^2 e/h^3 = 1.2 \times 10^6\ \mathrm{A\,m^{-2}\,K^{-2}}$ (m^*: the effective electron mass), T is the temperature in Kelvin, e indicates the electron charge, k: Boltzmann's constant = $1.38 \times 10^{-23}\ \mathrm{J\,K^{-1}} = 8.6 \times 10^{-5}\ \mathrm{eV\,K^{-1}}$, h: Planck's constant = $6.63 \times 10^{-34}\ \mathrm{J\,s} = 4.13 \times 10^{-15}\ \mathrm{eV\,s}$, Φ_0 indicates the potential barrier height (which does not depend on the voltage when the current is weak ($\Phi_{(v)} = \Phi_{(v=0)} = \Phi_0$) and decreases rapidly and significantly in the vicinity of the threshold voltage).

By determining the slope of the $\mathrm{Ln}\,[J] = f(E^{1/2})$ curve, we can also calculate the average width of a potential barrier at zero bias: $2\omega_0$, according to the following formula[17]:

$$\beta = \sqrt{\frac{e^3}{(4\pi\varepsilon_0\varepsilon_r n\omega_0)}} \Leftrightarrow \omega_0 = \frac{e^3}{(4\pi n_D \varepsilon_0 \varepsilon_r \beta^2)} \quad (6)$$

n stands respectively for the number of grains per unit length. ε_0 and ε_r are the permittivity of the vacuum and SnO_2 in the depletion region, respectively. A boundary might be represented as a sheet of trapped charge area density n_t, the barrier height Φ_0 is given as

$$\phi_0 = \frac{e^2 n_t^2}{8\varepsilon_o \varepsilon_r n_D} \quad (7)$$

and[1]

$$2\omega_0 = \frac{e n_t}{n_D} \quad (8)$$

where n_D is the carrier concentration in the grains. The former equations indicate that both barrier height as well as width should increase with decreasing grain conductivity.

Table 2 outlines the details of the electronic parameters describing the potential barrier of the specimen. Φ_0 (1.04 eV) does not show appreciable difference within the range 0.9–1 eV reported previously for tin oxide.[11] The values are of the same order of magnitude compared with those described when calculating the barrier of industrial ZnO-based varistors. The barrier height (Φ_0) is in fact about 0.7–0.8 eV for the most commercial varistors,[1,5,18] $n_D \sim 10^{23}\ \mathrm{m^{-3}}$, $n_t \sim 10^{16}$–$10^{17}\ \mathrm{m^{-2}}$ and $2\omega \sim 100$ nm.

3.2. Band conduction theory of SnO_2/SnO_2 junction

Fig. 3 depicts a SnO_2/SnO_2 junction as a double Schottky barrier appearing symmetric to a grain boundary of negligible thickness δ. The bottom of the conduction band is related to the Sn^{IV} cations ([Kr] $4d^{10}$) and probably empty $5s^0$ orbitals. The top of the valence band is associated with the p levels of the O^{2-} anion ([He] $2s^2 2p^2$). Fig. 3 superimposes, in fact, two diagrams of bands. The first concerns the junction with thermodynamic balance ($V = 0$), the second with the situation when the junction is subjected to a potential difference ($V_{gap} < V < 0$). In both cases, the periphery of each grain in contact with the grain boundary is deserted by the mobile charge carriers, i.e. the electrons of the conduction band. The electrons are trapped in the empty surface states at the grain boundaries. This displacement

Table 1
Densification before and after sintering (doped SnO_2 varistors with large range of operation sintered at 1623 K, during 2 h at a rate of 120 K h^{-1} up and down) and electrical parameters associated (non linear coefficient (α), threshold field ($E_{1mAcm^{-2}}$), leakage current density (J_f) and voltage per barrier (V_b), R_1 and R_2 stand, respectively, for the ratio U_{1kA}/U_{1mA} and U_{500A}/U_{1mA}).

Relative density before sintering (%) ±1	Relative density after sintering (%) ±0.02	Grain size repartition after sintering (mm) ±2	α ±12	$E_{1mAcm^{-2}}$ (V mm^{-1}) ±7	J_f (A cm^{-2}) $\pm 0.06 \times 10^{-9}$	V_b (V) ±0.5	R_1 ±0.01	R_2 ±0.01
64	98.8	10.4 ± 5	38	234	1.60×10^{-9}	2.5	2.16	1.97

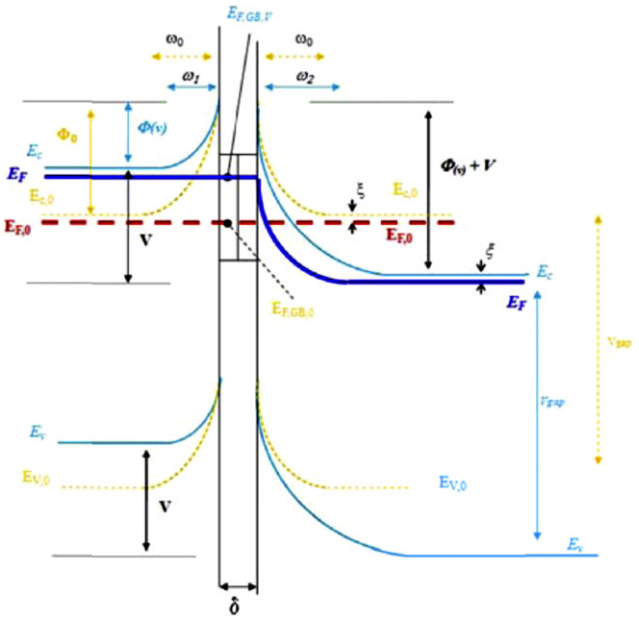

Fig. 3. Energy band diagram for a double Schottky barrier formed at the interfaces of the system: *SnO_2 grain – grain boundary – SnO_2 grain* without and with a potential difference perpendicular to the boundary. At equilibrium or null tension, the Fermi level in the grains and the grain boundary are equal. Under the effect of a potential difference V, bands are deformed. The Fermi level in the left grain is increased and lowered in the grain of right-hand side. The surface bands are schematised by rectangles. SnO_2 is regarded as a degenerated semiconductor, i.e. the Fermi level is at least 3 kT below the conduction band. (ξ indicates the difference in energy level between the Fermi level and the level corresponding to the bottom of the conduction band). Index "0" and the writing in *italic* refer to the diagram for a null tension, the thickness of the grain boundary $\delta \ll \omega_0$ and $2\omega_0 = \omega_1 + \omega_2$. Surface states corresponding to each grain are schematised by a rectangle and the Fermi level associated relating to the situation at equilibrium and at non equilibrium is deferred as $E_{F,GB,0}$ and $E_{F,GB,v}$.

of charge carriers led to a decrease in the number of free electrons in the conduction band. As a result it moves away from the Fermi level, which remains horizontal at thermodynamic equilibrium. In other words, at equilibrium, the Fermi level of the two adjacent grains is the same since there is no net current flow.

A quantitative description of the double Schottky barrier in Fig. 3 can be established by solving Poisson's equation in its one-dimensional form. By assuming a continuous charge distribution in the depleted region, whose maximum thickness is about 200 nm,[19] we obtain for a given thermodynamic temperature T:

$$\frac{d^2V}{dx^2} = -\frac{en_T}{\varepsilon_0\varepsilon_r} \quad (9)$$

where V indicates the negative electric potential deferred on Fig. 3, n_T is the total charge density in the vicinity of the grain boundary:

$$n_T = n_D - n_A - n + p \quad (10)$$

A rigorous inventory of the charge carriers gives:

n_D: density of positive static charges or density of donors assuming that at room temperature all the atoms are ionised,
n_A: density of negative static charges or density of acceptors if all the atoms are ionised,
n: density of negative charge carriers (electrons in the conduction band),
p: density of positive charge carriers (holes in the valence band).

SnO_2 ceramics nearly always exhibit strong n-type semiconductivity, with electrons in the conduction band as the charge carriers. Non-stoichiometric tin oxide ($SnO_{2-\delta}$; $\delta = 0.03$) appearing above 1173 K[20] has traditionally been attributed as the origin of the conductivity since the formation of a vacancy (written as $V^{\bullet\bullet}_O$ in the Kröger–Vink notation) might free two electrons (e') in the conduction band: $O^x_O = 2\,e' + V^{\bullet\bullet}_O + 1/2O_2$ (g). However, it seems that the conductivity measured at room temperature cannot be linked to such point defects because their concentrations are not high enough at room temperature. Extrinsic defects such as hydrogen incorporated unintentionally might be a candidate.[21,22] Ab initio calculations show that hydrogen acts always as a shallow donor in SnO_2. However since our specimens are intentionally doped with several additives, we have assumed that the native shallow donors are secondary compared with the bulk contribution of the added donors.

Among the additives incorporated in this composition, positively charged donors might diffuse into SnO_2 grains and free

Table 2
Electrical parameters describing a doped-SnO_2 varistors with large range of operation (barrier energy (Φ_0), half width of the potential barrier (ω_0), charge carrier concentration (n_D), trapped charge area density (n_t), apparent conductivity of the grain boundaries (σ_{gb}) and conductivity of the grains (σ_g).

Varistor	ϕ_0 (eV) ±0.02	ω_0 (m) $\pm 4 \times 10^{-9}$	n_D (m^{-3})	n_t (m^{-2})	σ_{gb} (S m^{-1})	σ_g (S m^{-1}) ±0.4
Doped-SnO_2	1.04	6×10^{-9}	$(3.0 \pm 0.3) \times 10^{25}$	$(3.7 \pm 0.2) \times 10^{17}$	$(2.5 \pm 0.5) \times 10^{-10}$	207.6
Doped-ZnO	0.90	11×10^{-9}	$(7.3 \pm 0.7) \times 10^{24}$	$(1.59 \pm 0.09) \times 10^{17}$	$(1.4 \pm 0.2) \times 10^{-8}$	111.2

electrons to the conduction band associated with the grains. For instance, pentavalent tantalum might free electrons within the conduction band:

$$Ta_2O_5 \xrightarrow{SnO_2} Ta^{\bullet} + e'$$

Other dopants such as cobalt might create acceptor states in the SnO_2 band gap such as

$$Co^{\bullet\bullet} \rightarrow Co''_{Sn} + 2h^{\bullet},$$

$h^{\bullet}$: being a hole in the Kröger–Vink notation.

Other charge acceptors might include: Co"$_{Sn}$, Cr'$_{Sn}$, B'$_{Sn}$, Al'$_{Sn}$, Tl'$_{sn}$ (intrinsic defects such as V'$_{Sn}$, V"$_{Sn}$, O' and O" might also be present as acceptors)[18].

Generally, the resolution of Poison's equation is carried out by assuming that $n_T \sim n_D$:

1. Doping atoms are all ionised.
2. There are sharp boundaries at the edges defining the donor and trap regions, with no spill-over from free charge carriers.
3. A plane two-dimensional interface with a net trapped charge located at the surface of each grain: Q_s.
4. SnO_2 grains are primarily composed of donor atoms: $n_A \ll n_D$.
5. Electrons in the vicinity of the grain boundary have deserted the area: $n \rightarrow 0$.
6. Ultimately the minority charge carriers are neglected compared with the electrons: $n \gg p$.

Under the latter conditions, integration of Poisson's equation allows us to estimate the quantity of space charges:

$$Q_{space} = en_D 2\omega_0 = (8\varepsilon_0\varepsilon_r en_D \Phi_{(v)})^{1/2} \quad (11)$$

$$2\omega_0 = 2\frac{(2\varepsilon_0\varepsilon_r\Phi_{(v)})^{1/2}}{en_D} \times (2\,\omega_0 \text{ being the thickness of the depletion layer}) \quad (12)$$

Dorlanne and Tao[19] carries out calculations without approximations concerning the minority charge carriers. The formula obtained thus differs slightly from that which is commonly retained (11):

$$Q_{space} = (2\varepsilon_0\varepsilon_r en_D)^{1/2}(\Phi_{(v)}^{1/2} + (\Phi_{(v)} + V)^{1/2}) \quad (13)$$

Note that for zero potential, (13) converges towards (12).

Charge conservation states that the electronic charge trapped on the surface, Q_s, is equal to the space charge previously calculated:

$$Q_s = n_s\, e = Q_{space}$$

The surface density of electrons trapped on the surface of the grain boundary is therefore:

$$n_S = \left(\frac{8\varepsilon_0\varepsilon_r n_D \Phi_0}{e}\right)^{1/2} \quad (14)$$

Dorlanne and Tao[19] also calculate an expression of the surface charges independently of that of the space charge:

$$Q_s = Q_{s,0}\left(1 + \frac{V}{2V_{gap}}\right) \quad (15)$$

$Q_{s,0}$: being the surface charge for $V = 0$ V.

From (13) and (15), two equations are deduced:

- Neglecting the minority charge carrier, only the majority charge carriers are considered:

$$\left(\frac{e\Phi_{(v)}}{kT}\right)^{1/2} + \left(\frac{e(\Phi_{(v)} + V)}{kT}\right)^{1/2} - 2\left(\frac{e\Phi_0}{kT}\right)^{1/2}\left(1 + \frac{V}{2V_{gap}}\right) = 0 \quad (16)$$

- Without approximation on the charge carrier, both majority and minority charge carriers are considered:

$$\left(\frac{e\Phi_{(v)}}{kT} + \exp^{(-e\Phi_{(v)}/kT)} - 1\right)^{1/2} + \left(\frac{e(\Phi_{(v)} + V)}{kT} + \exp^{(-e(V_{gap}-\Phi_{(v)}-V)/kT)} - 1\right)^{1/2} = -2\left(\frac{e\Phi_{(0)}}{kT} - 1\right)^{1/2}\left(1 + \frac{V}{2V_{gap}}\right) = 0 \quad (17)$$

Eq. (17) cannot be solved analytically. However it can be used to determine $\phi_{(v)}$ numerically as a function of V taking into account the experimental data: $\phi_0 = 1$ eV and $V_{gap} = 3.7$ V at 300 K. The potential barrier of 0.9 eV–1 eV is evaluated starting from our own experimental values which converge towards those reported recently by Glot et al.[26], who extracts the height of barrier starting from the slope of the Arrhenius diagram # ($\mathrm{Ln}\,(j/AT^2)$ versus $1/T$). It is worth noticing that $\phi_{(\mathbf{v})}$ versus V is possible only if the product # $T\,\mathrm{d}\Phi_{(v)}/\mathrm{d}T$ is negligible compared with $\phi_{(\mathbf{v})}$. If we consider the thermionic current even in its simplest form ($J = AT^2\exp^{(-e\Phi/kT)}$):

$$\frac{\mathrm{d}\,\mathrm{Ln}\,(J/AT^2)}{\mathrm{d}(1/T)} = -\frac{e}{k}\left(\Phi - T\frac{\mathrm{d}\Phi}{\mathrm{d}T}\right) \quad (18)$$

The theoretical potential barrier at the interface according to the applied potential ($\phi_{(\mathbf{v})}$ versus V) is shown on Fig. 4. The decrease of $\phi_{(v)}$ starting from Eq. (17) tends towards zero for a voltage corresponding to that of the forbidden band: V_{gap}.

In addition, the potential barrier decay with applied voltage proceeds in two stages. The height of the potential barrier first drops, then eventually collapses near V_{gap}: $\mathrm{d}(\phi_{(v)}/\mathrm{d}V) = -0.864\,\mathrm{eV\,V^{-1}}$. The sudden decrease in $\phi_{(v)}$ for V greater than 3 V is a direct consequence of the sudden emergence of holes, within the right hand grain. The barrier collapses in accordance with Eq. (17). It is therefore quite possible to consider the holes effect without assuming about their movement, considering only their influence on the global amount of charge as varying with V. The physical process responsible for the appearance of the holes is therefore not explained but the

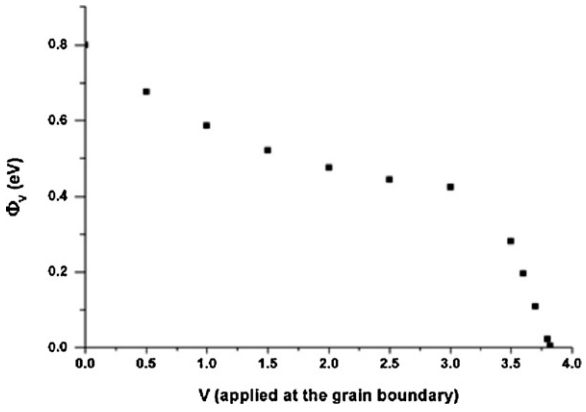

Fig. 4. Theoretical evolution of the potential barrier, $\phi_{(v)}$, according the potential applied to the grain boundary of a SnO_2 varistor. The drop of $\phi_{(v)}$ comes from the exponential increase in the holes number in the right-hand side grain when $\phi_{(v)} + V = V_{gap}$; $V \sim 3.7$ V.

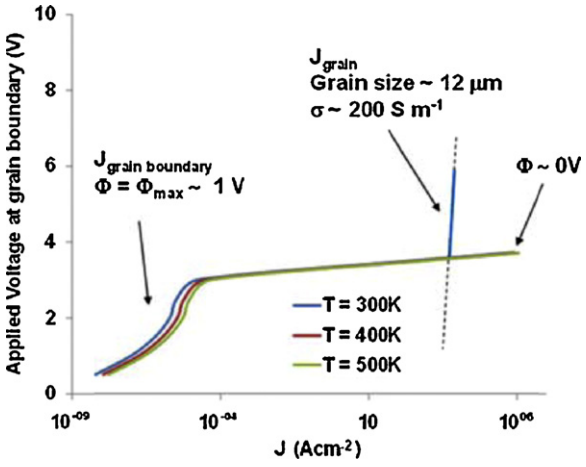

Fig. 5. Full simulation of a SnO_2/SnO_2 junction.

model makes it possible to give an account of the sudden increase in α when entering the region of non-linearity and in particular of non-linear coefficients greater than 100.

The theoretical influence of the voltage on the non-linearity coefficient is estimated starting from the simple expression of a thermionic current (or thermal electron emission), i.e. heat-induced flow of charge carriers from the SnO_2 grain surface or over the potential-energy barrier at grain boundary:

$$j = AT^2 \exp\left(\frac{-\Phi_{(v)}}{kT}\right) \tag{19}$$

A is the Richardson constant: $A = 4\pi m * k^2 e/h^3$, h and k Planck's and Boltzmann's constant, respectively, and m^* the effective mass of an electron in the depletion layer of SnO_2 (we assumed that the electrons behave in many respects as if they were free in a single SnO_2 crystal and in the depletion layer).

Eq. (19) indicates that as soon as the temperature exceeds 0 K a current appears. In the case of varistors, the current is governed by field enhanced thermionic emission. The general equation is then:

$$j = AT^2 \exp^{(-(\Phi - \Delta\Phi)/kT)} \tag{20}$$

To obtain a net DC current flow across the interface we need to correct for the current flow in the opposite direction which is suppressed by a factor $\exp(-eV/kT)$, and for the current that is trapped and re-emitted at the interface. The latter correction is however considered as negligible for the capture cross-sections for electrons.[7] The total current density which describes the flow of electrons passing over the top of the electrostatic barriers is[1]:

$$j = AT^2 \exp^{(-(e\Phi_{(V)} + \xi)/kT)} \exp^{(-eV/kT)} \tag{21}$$

ξ: difference in energy between the Fermi level (E_F) and the bottom of the conduction band (E_C), $\xi = E_F - E_C \sim 0.13$ eV for ZnO[6,23] (Fig. 3).

In order to estimate the electric field to which the grain boundary is exposed, we assumed a depletion zone width of 200 nm (200×10^{-6} mm). Fig. 5 shows the theoretical thermal dependence of the change in current density against voltage. A positive dependence is found in agreement with experimental data. Moreover, it is worth nothing that in agreement with experience when the applied field reaches the breakdown field of the SnO_2 grain boundary, there is no further temperature dependence.

3.3. Discussion

Fig. 5 also shows using Ohm's law $J = \sigma V/l$, l being the average grain size (12 µm), the upturn region for a SnO_2–SnO_2 junction. The conductivity of the doped grain is assumed to be equal to 200 S m^{-1} in agreement with our experimental results. Note that for $\Phi = 0$ at 3.82 V the current density in the grain boundary ($J_{gb} = 2 \times 10^8$ A m^{-2} or 2×10^4 A cm^{-2}) is higher than the current in the grains ($J_g = 8 \times 10^7$ A m^{-2} or 8×10^3 A cm^{-2}).

It is remarkable that the appearance of the holes occurs for a voltage directly related to the forbidden band. The value of the threshold voltage therefore mainly depends on the forbidden band and not addition of any element: $V_{gap} = 3.3$ V for ZnO and 3.7 V for SnO_2. This theoretical analysis on the level of a grain boundary should not, however, make us forget the macroscopic complexity of polycrystalline ceramics. In such media, the joints are laid out in a three-dimensional arrangement with variable behaviour of one joint with respect to another.[24,25] Also the apparent dispersion of electric values of characteristics observed on the varistors may lie not only in the effective quality of the barriers but also in the degree of heterogeneity of the materials elaborated. The lower the percentage of bad joints, the greater the macroscopically non-linear varistor effect.

This suggests that the region of varistor operation is less conditioned by the electronic parameters defining the potential barrier, i.e. the charge carrier density, surface trapped charge density and the height of the potential barrier, than by the effective area of the grain boundaries. Indeed, this parameter is determining when calculating the current density. However, the effective area of a grain boundary is not easy to measure. The presence of segregation in the grain boundary probably actuates barriers (voltage independent) which limit the current density to high electric field.

3.4. Comparison of the model

Glot et al.[26] established in experiments that electric conduction in varistors containing SnO_2 is controlled by the potential barriers present at the grain boundaries and non-ohmic conduction is due to the collapse of the potential barrier under the action of the increase in the electric field. A semi-empirical expression is proposed to illustrate the dependence of the electrical conduction activation energy:

$$E_{\sigma,E} = E_{\sigma,0} - \left|\frac{d\Phi_{(v)}}{dE}\right| E \quad (22)$$

where $E_{\sigma,0}$ is the electrical conduction activation energy at the low electrical field in the ohmic region. Thus, the electrical conduction activation energy is linearly decreased with electrical field if the rate of change of the barrier height on electrical field is constant.

The electrical conduction activation energy as a function of the electrical field E is obtained experimentally and correlated to the nonlinear coefficient. Experimental dependence clearly exhibits a low field part with low slope and a high field part with higher slope. The first slope is attributed to a thermally activated conduction process, the higher slope is related to the contribution of minority carriers (holes). Glot's experimental data are in agreement with Fig. 4 which shows the theoretical change in the potential barrier with the potential applied to the grain boundary.

Parra et al. and Ponce et al.[16,27] have reported studies on the conduction modes in SnO_2 varistors where they show that the tunnelling conduction cannot be neglected. They first measured the capacitance of the ceramics (C) experimentally at frequencies above 100 kHz at 423 K, from which the barrier height and donor concentration are calculated from the traditional equation (neglecting minority charge carriers):

$$\frac{1}{C} = 2\left(\frac{2\Phi n^2}{e^2\varepsilon_0\varepsilon_r n_D S^2}\right)^{1/2} \quad (23)$$

and

$$\Phi = -kT\,\mathrm{Ln}\left(\frac{V}{S\,R_{gb}AT^2}\right) \quad (24)$$

where n is the average number of grains across the specimen thickness, S the area of the electrodes, V the applied voltage during impedance spectroscopy measurements and R_{gb} the grain boundary resistance measured at frequencies below 100 Hz.

Hence, knowing the barrier height a thermionic current density: $J_{\mathrm{thermionic,423K}}$ is calculated.

In a second approach, the total current is assumed to be due to both tunnelling and thermionic emission. An expression of the total current is therefore given where a Fermi–Dirac distribution and a transmission probability for a reverse-biased Schottky barrier are displayed: $J_{\mathrm{total}} = J_{\mathrm{thermionic}}\,(\Phi) + J_{\mathrm{tunnel}}\,(\Phi, N_d)$.

Iterative calculations were carried out until the calculated total current density was equal to the current density calculated in the case of a purely thermionic mechanism:

$$J_{\mathrm{thermionic}} + J_{\mathrm{tunnel}} = J_{\mathrm{thermionic,423K}}.$$

Our experimental data are similar and following the calculations proposed by Ponce et al.[27] we found that the tunnel and thermionic conductions made similar contributions at 298 K. The result is difficult to interpret. However, this result might be not surprising since we extract parameters from classical equations of thermionic conduction where minority charge carriers are neglected.

3.5. Non-ohmic conduction in ZnO and SnO_2 system

In spite of numerous exploratory works, only both zinc and tin oxides present such high non-linearity effects (>40). Such high non linearity values are thought to result from an impact ionisation process.

If there is a common origin of polycrystalline ceramic varistors of doped-ZnO and doped-SnO_2 the most probable candidate is oxygen (hydrogen being ruled out). Hydrogen is likely to adsorb and diffuse along or inside the grain boundaries. But its role in promoting impact ionisation process in large bandgap ZnO and SnO_2 still remains unclear.

4. Conclusion

In conclusion, SnO_2 varistors, correctly doped, exhibit large and similar range of operation as commercial ZnO varistors. The similarity of the electrical behaviour of doped dioxide and doped ZnO ceramics is demonstrated through a theoretical model which contains no adjustable parameters. Only two intrinsic material constants are involved: the band gap and the height of the potential barrier. This approach shows that a thermoelectric mechanism explains the experimental results without a contribution of a tunnelling mechanism. The participation of minority carriers in the total amount of charge induces a significant decrease in barrier height, leading to a sharp increase in the thermoelectric current over the barrier. For highly nonlinear ceramics, impact ionisation occurs. This phenomenon contributes further to the barrier height decay.

A limitation of this double Schottky barrier model is that it only describes the charge carrier transport across a single interface. When considering the varistor as a whole, it is necessary to account for the fact that the varistor consists of a large number of grain boundaries with individual properties.

Acknowledgement

Thanks to the funding of the French National Research Agency (ANR) through the research project "Eco-parafoudres".

References

1. Clarke D. Varistor ceramics. *Journal of the American Ceramic Society* 1999;**82**(3):485–502.
2. Pianaro SA, Bueno PR, Longo E, Varela JA. A new SnO_2-based varistor system. *Journal of Materials Science Letters* 1995;**14**:692–4.
3. Glot AB, Zlobin AP. Nonohmic conductivity of ceramics based on tin dioxide. *Neorganicheskie Materialy* 1989;**25**(2):322–4.

4. Rossinelli M, Greuter F, Schmuckle F. Electrically active grain boundaries in ceramics: varistors and capacitors. *British Ceramic Proceedings* 1989;**41**:177–82.
5. Stucki F, Bruesch P, Greuter F. Electron spectroscopic studies of electrically active grain boundaries in ZnO. *Surface Science* 1987;**189/190**:294–9.
6. Blatter G, Greuter F. Carrier transport through grain boundaries in semiconductors. *Physical Review B* 1986;**33**:3952–66.
7. Greuter F, Blatter G. Electrical properties of grain boundaries in polycrystalline compound semiconductors. *Semiconductor Science and Technology* 1990;**5**:111–37.
8. Sato Y, Yamamoto T, Iuhara Y. Atomic structures and electrical properties of ZnO grain boundaries. *Journal of the American Ceramic Society* 2007;**90**(2):337–57.
9. Fan J, Freer R. Deep level transient spectroscopy of SnO_2-based varistors. *Applied Physics Letters* 2007;**90**:093511–93513.
10. Pansiot J. Elaboration, characterization and simulation of new tin dioxide based varistors, Ph.D. dissertation, 32-2010, University of Lyon 1, Lyon, 2010.
11. Metz R, Morel J, Houabes M, Pansiot J, Hassanzadeh M. High voltage characterization of tin oxide varistors. *Journal of Materials Science* 2007;**42**(24):10284–7.
12. Lu Z-Y, Chen Z, Wu J-Q. SnO_2-based varistors capable of withstanding surge current. *Journal of the Ceramic Society of Japan* 2009;**117**(7):851–5.
13. Fayat J, Castro MS. Defect profile and microstructural development in SnO_2-based varistors. *Journal of the European Ceramic Society* 2003;**23**:1585–91.
14. Mendelson MI. Average grain size in polycrystalline ceramics. *Journal of the American Ceramic Society* 1969;**52**(8):443–6.
15. Glot AB. Ceramic materials research trends. In: Lin PB, editor. *Hauppauge*. New York: Nova Science; 2007. p. 227–73.
16. Parra R, Ponce MA, Aldao CM, Castro MS. Advances in the study of the conduction modes in SnO_2 varistors. *Journal of the European Ceramic Society* 2007;**27**:3907–9.
17. Antunes AC, Antunes SRM, Pianaro SA, Longo E, Leite ER, Varela JA. Effect of La_2O_3 doping on the microstructure and electrical properties of a SnO_2 based varistor. *Journal of Materials Science: Materials in Electronics* 2001;**12**:69–74.
18. Bueno P, Varela J, Longo E. SnO_2, ZnO and related polycrystalline compound semiconductors: an overview and review on the voltage-dependent resistance (non-ohmic) feature. *Journal of the European Ceramic Society* 2008;**28**:505–29.
19. Dorlanne O, Tao M. The grain junction in zinc oxide varistors. *Materials Science Monographs (High Tech Ceram, Pt B)* 1987;**38B**:1809–17.
20. Mizusaki J, Koinuma H, Shimoyama JI, Kawasaki M, Fueki K. High temperature gravimetric study on nonstoichiometry and oxygen adsorption of SnO_2. *Journal of Solid State Chemistry* 1990;**88**:443–50.
21. Robertson J, Peacock PW. Doping and hydrogen I wide gap oxides. *Thin Solid Films* 2003;**445**:155–60.
22. Samson S, Fonstad CGJ. Defect structure and electronic donor levels in stannic oxide crystals. *Journal of Applied Physics* 1973;**44**: 4618–21.
23. Manuel PA. Mecanismes de conduction et de dégradation dans les varistances ZnO. *Revue de Physique Appliquée* 1987;**22**(9):971–9.
24. Tao M, Ai B, Dorlanne O. The grain junction in zinc oxide varistors. *Journal of Applied Physics* 1987;**61**(4):1562–7.
25. Dorlanne O, Ai B, Destruel P, Loubière A. Electrical characteristics of zinc oxide varistors subjected to hydrostatic pressure. *Journal of Applied Physics* 1985;**57**(12):5535–8.
26. Glot AB, Gaponov AV, Sanoval-Garcia AP. Electrical conduction in SnO_2 varistors. *Physica B* 2010;**405**:705–11.
27. Ponce MA, Ramirez MA, Parra R, Malagu C, Castro MS, Bueno PR, Varela JA. Influence of degradation on the electrical conduction process in ZnO and SnO_2-based varistors. *Journal of Applied Physics* 2010;**108**: 074505–74509.